Journal of Applied Physics

Size effects in the magnetic properties of ε-Fe_2O_3 nanoparticles

Cite as: J. Appl. Phys. **118**, 213901 (2015); https://doi.org/10.1063/1.4936838
Submitted: 15 July 2015 . Accepted: 18 November 2015 . Published Online: 01 December 2015

A. A. Dubrovskiy, D. A. Balaev, K. A. Shaykhutdinov, O. A. Bayukov, O. N. Pletnev, S. S. Yakushkin, G. A. Bukhtiyarova, and O. N. Martyanov

Size effects in the magnetic properties of ε-Fe_2O_3 nanoparticles

A. A. Dubrovskiy,[1,2,a)] D. A. Balaev,[1,3] K. A. Shaykhutdinov,[1] O. A. Bayukov,[1] O. N. Pletnev,[1] S. S. Yakushkin,[4,5] G. A. Bukhtiyarova,[4] and O. N. Martyanov[4,5]
[1]*Kirensky Institute of Physics, Krasnoyarsk 660036, Russia*
[2]*International Laboratory of High Magnetic Fields and Low Temperatures, Wroclaw 53-421, Poland*
[3]*Siberian Federal University, Krasnoyarsk 660041, Russia*
[4]*Boreskov Institute of Catalysis, Novosibirsk 630090, Russia*
[5]*Novosibirsk State University, Novosibirsk 630090, Russia*

(Received 15 July 2015; accepted 18 November 2015; published online 1 December 2015)

We report the results of comparative analysis of magnetic properties of the systems based on ε-Fe_2O_3, nanoparticles with different average sizes (from ∼3 to 9 nm) and dispersions. The experimental data for nanoparticles higher than 6–8 nm in size are consistent with the available data, specifically, the transition to the magnetically ordered state occurs at a temperature of ∼500 K and the anomalies of magnetic properties observed in the range of 80–150 K correspond to the magnetic transition. At the same time, Mőssbauer and ferromagnetic resonance spectroscopy data as well as the results of static magnetic measurements show that at room temperature all the investigated samples contain ε-Fe_2O_3 particles that exhibit the superparamagnetic behavior. It was established that the magnetic properties of nanoparticles significantly change with a decrease in their size to ∼6 nm. According to high-resolution electron microscopy and Mőssbauer spectroscopy data, the particle structure can be attributed to the ε–modification of trivalent iron oxide; meanwhile, the temperature of the magnetic order onset in these particles is increased, the well-known magnetic transition in the range of 80–150 K does not occur, the crystallographic magnetic anisotropy constant is significantly reduced, and the surface magnetic anisotropy plays a decisive role. This is apparently due to redistribution of cations over crystallographic positions with decreasing particle size, which was established using Mössbauer spectra. As the particle size is decreased and the fraction of surface atoms is increased, the contribution of an additional magnetic subsystem formed in a shell of particles smaller than ∼4 nm becomes significant, which manifests itself in the static magnetic measurements as paramagnetic contribution. © *2015 AIP Publishing LLC*.
[http://dx.doi.org/10.1063/1.4936838]

I. INTRODUCTION

Trivalent iron oxide ε-Fe_2O_3 characterized for the first time in 1998 (Ref. 1) has unique properties and can find wide applications.[2,3] This oxide exists in the form of nanoparticles up to 25–100 nm in size with a significant (∼20 kOe) room-temperature coercivity,[2–5] which makes these particles promising for application in magnetic recording. In addition, this material exhibits the magnetoelectric effect.[6] It was demonstrated that ε-Fe_2O_3 nanoparticles effectively absorb microwave radiation in the millimeter range.[7,8] By now, there has been a lack of a commonly held opinion concerning the ε-Fe_2O_3 magnetic structure around room temperature.[2,3] Judging by the magnetic properties, it can be a collinear ferrimagnet or a canted antiferromagnet. According to the data of magnetic measurements and neutron study, the effective magnetic moment per Fe^{3+} atom is ∼0.3 μ_B (Refs. 4, 5, 9, and 10) and the transition to the magnetically ordered state occurs near ∼500 K.[2–13] In the temperature range of 80–150 K, the ε-Fe_2O_3 oxide undergoes a magnetic transition accompanied by anomalies in the magnetic properties and leading to a significant decrease in the coercivity. The nature of this transition is still argued.[2,3]

The magnetic properties and resonance behavior of ε-Fe_2O_3 are modified upon partial substitution of Al,[14] Ga,[7] or In[8,15,16] for Fe. On the other hand, the properties can change with decreasing particle size and increasing fraction of surface atoms. A decrease in the particle size can lead to (i) redistribution of cations over ε-Fe_2O_3crystallographic positions, (ii) the related variation in the bulk magnetic anisotropy of ε-Fe_2O_3 particles and the influence of surface magnetic anisotropy, and (iii) the superparamagnetic (SP) state, in which magnetic moments of particles are unblocked in a wide temperature range.

In Refs. 17 and 18, it was proposed to synthesize ε-Fe_2O_3 nanoparticles on silica gel by incipient wetness impregnation with the Fe(II) sulphate solutions. This technique allowed obtaining for the first time the systems of ε-Fe_2O_3 particles with an average size of few nanometers without any other iron oxide polymorphic phases, which is much smaller than in the above-cited studies. Study of the magnetic properties of the synthesized samples showed that they exhibit the SP behavior[19,20] and the magnetic properties of small (<6 nm) particles reveal no anomalies typical of coarser ε-Fe_2O_3 particles.[20] Meanwhile, study of the dynamic magnetization reversal (magnetic hysteresis in a pulsed magnetic field) of ε-Fe_2O_3 particles with the size $d \sim 10$ nm showed that the effective coercivity grows with

a)E-mail: andre-do@yandex.ru

the field variation rate.[21] This effect originates from relaxation of SP particles[22,23] and the surface anisotropy significantly contributes to these processes.

Critical volume V (at a specified temperature) or blocking temperature T_B (for this volume) at which the SP state is established can be estimated using the Néel–Brown formula

$$T_B = K_{eff} V / \ln(\tau/\tau_0) k. \quad (1)$$

Here, K_{eff} is the effective magnetic anisotropy constant, which involves bulk magnetic anisotropy K_V and the surface contribution to the magnetic anisotropy; k is the Boltzmann constant; τ is the characteristic observation (measuring) time; and τ_0 is the time of SP relaxation of a particle. The τ_0 values usually lie within 10^{-13}–10^{-9} s and measuring time τ depends on the experimental technique used; e.g., $\tau_{sm} \sim 10^1$–10^2 s for static magnetic measurements and $\tau_M \sim 10^{-9}$–10^{-8} s for Mössbauer spectroscopy.[24] As particle size D is decreased, the increasing role is played by the surface magnetic anisotropy, which, in the simplest case, is taken into account as[25]

$$K_{eff} = K_V + 6K_S/D, \quad (2)$$

where K_S is the surface magnetic anisotropy constant.

In this study, we compare the data obtained using static magnetization measurements and Mössbauer and ferromagnetic resonance (FMR) spectroscopy for samples with different average particle sizes and dispersions of the size distribution of particles in order to establish the size at which particles exhibit the SP behavior at different experimental techniques and to estimate the bulk and surface magnetic anisotropy in small ε-Fe_2O_3 particles.

II. EXPERIMENT

A. Sample preparation and size distribution of particles

The ε-Fe_2O_3 particles were synthesized on the surface of the silica gel using wet chemical pore filling impregnation method with Fe^{2+} sulphate solutions and subsequent drying at the temperature $T = 110\,^\circ$C and tempering at 900 °C for 4 h.[17,18] A Khromanalyt KSKG silica gel matrix with a specific surface area of 287 m^2/g, an average pore radius of ~141 Å, and a pore volume of ~0.35 cm^3/g was used. The silica gel grain size was from 0.25 to 0.5 mm. As was shown in Ref. 26, the ε-Fe_2O_3 phase starts forming at temperatures around 600 °C; at 900 °C, the content of this phase attains its maximum. We investigated three types of the samples with iron ion concentrations of about 0.74, 3.4, and 7.4 wt. %, hereinafter referred to as 05FS, 3FS, and 7FS, respectively.

Analysis of X-ray diffraction data (XRD) proves the ε-Fe_2O_3 phase in of 3FS and 7FS samples without any impurities (within the XRD accuracy of ~5%) of foreign polymorphs of iron oxide.[18] To check the purity of the samples (especially the 05FS sample), we made additional analysis using Mössbauer spectroscopy. The detection of tetrahedral and octahedral positions of cations in superparamagnetic phase and forming of the ε-oxide-type Mössbauer spectra gives us possibility to regard the superparamagnetic phase as the precursor of ε-oxide. The absence of the sextets, which are equivalent to γ-Fe_2O_3 (~500 kOe) and α-Fe_2O_3 (~517 kOe) proves negligible quantity of them, see p.p.3.1 for details.

High-resolution transmission electron microscopy (HRTEM) investigations were performed on a JEOL JEM-2010 microscope operating at 200 kV accelerating voltage and ensuring resolution of up to 1.4 Å. The particle size distribution was estimated by a statistical count of particles from several frames taken from different sample parts.

According to HRTEM, all the samples contain near spherical iron oxide particles on the silica support.[18,19] Figure 1 presents HRTEM histograms of particle size distribution for samples 7FS, 3FS, and 05FS. It can be seen that sample 7FS has rather a broad particle size distribution: along with fine (below ~6 nm) particles, it contains coarse particles ~25 nm in size. Sample 3FS also contains a significantly large amount of particles smaller than ~6 nm, along

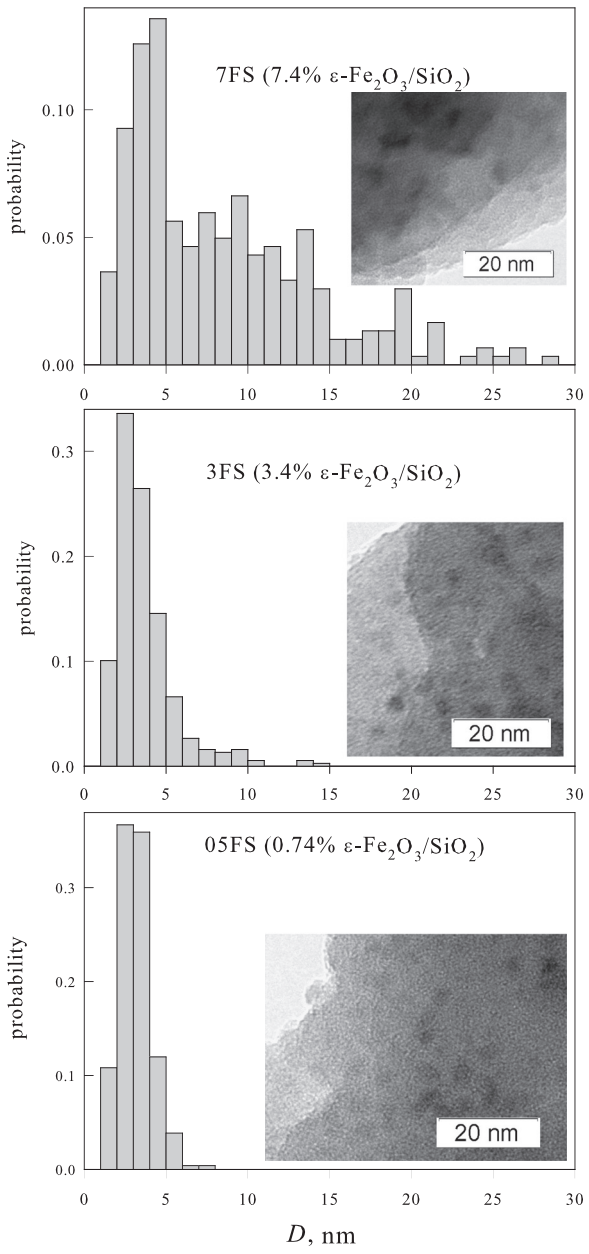

FIG. 1. Particle size distribution histograms with HRTEM images for the investigated samples. The average particle sizes are ~3.1 ± 1.0, 3.7 ± 2.3, and $\langle D \rangle$ ~8.6 ± 6.2 nm for samples 05FS, 3FS, and 7FS, respectively.

with larger particles up to 15 nm in size. In sample 05FS, most of particles are smaller than 6 nm, so the size distribution is rather narrow. Thus, the comparative analysis of the properties of these samples makes it possible to study size effects characteristic of small (below ~6 nm) ε-Fe_2O_3 particles, while the presence of particles ~20 nm in size in sample 7FS allows comparing the magnetic properties with the available literature data.

B. Techniques for studying the magnetic properties

The static magnetic properties were investigated using a vibrating sample magnetometer with the temperature range of 4.2–300 K (Ref. 27) a Quantum Design PPMS-6000 system with the temperature range from 300 to 850 K. Temperature dependences of magnetic moment $M(T)$ were obtained in the zero field cooled (ZFC) and field cooled (FC) regimes. Experimental magnetic moments were normalized to the Fe_2O_3 mass.

Mössbauer measurements were performed on an MC-1104Em spectrometer with a Co^{57}(Cr) source at room temperature (300 K) and liquid helium temperature (4.2 K).

Ferromagnetic resonance spectra were recorded on a Bruker ELEXSYS 500 spectrometer operating in the X-range with a characteristic microwave radiation frequency of ~10 GHz using a high-temperature attachment for operation at temperatures of 100–500 K.

III. RESULTS AND DISCUSSION

A. Mössbauer spectroscopy

Mössbauer spectra for samples 7FS, 3FS, and 05FS (Fig. 2) represent a sum of overlapping quadrupole doublets and Zeeman sextets. The parameters of sextets for the samples 7FS and 3FS are typical of Fe^{3+} ions in the ε-Fe_2O_3 phase. Small peaks on the spectrum wings for sample 7FS (Fig. 2(a)) correspond to the hematite impurity (~1% of the total iron amount). The quadrupole doublets correspond to the sample part, which is in the SP state at this temperature. The Zeeman sextets belong to the magnetically ordered sample part. It can be seen in Fig. 2(b) that upon cooling to 4.2 K all iron in samples 7FS and 3FS passes to the magnetically ordered state. A part of sample 05FS remains in the SP state up to the lowest temperatures.

The room-temperature spectra are developed against the background of a wide open trough containing nearly continuous assembly of the hyperfine fields. The probabilities of ultrafine fields P(H) in the experimental spectra (Fig. 3) are widely distributed in a wide field range. The through is apparently related to the part of particles in which the magnetic moment relaxation time is comparable with the relaxation time for a nuclear spin, and to surface cations with different degrees of exchange coupling with inner cations of particles. The Mössbauer parameters for the investigated samples are given in Table I, where the through is approximated by a wide singlet, Fe1–Fe3 are the octahedral positions of iron, Fe4 is the tetrahedral position of iron, and SP(B) and SP(A) are the octahedral and tetrahedral components of the SP phase. At the temperature $T = 4.2$ K, it is difficult to distinguish crystallographic positions in the spectra because of overlap of neighboring sextets; therefore, the spectra are approximated by a sum of two sextets corresponding to the octahedral (Fe(B)) and tetrahedral (Fe(A)) iron positions.

The ε-Fe_2O_3 unit cell[4] contains 24 octahedral positions, only 12 of which are occupied by iron, and 36 tetrahedral positions, only 4 of which are occupied. Tronc *et al.*[1] considered the possibility of different distributions of iron over

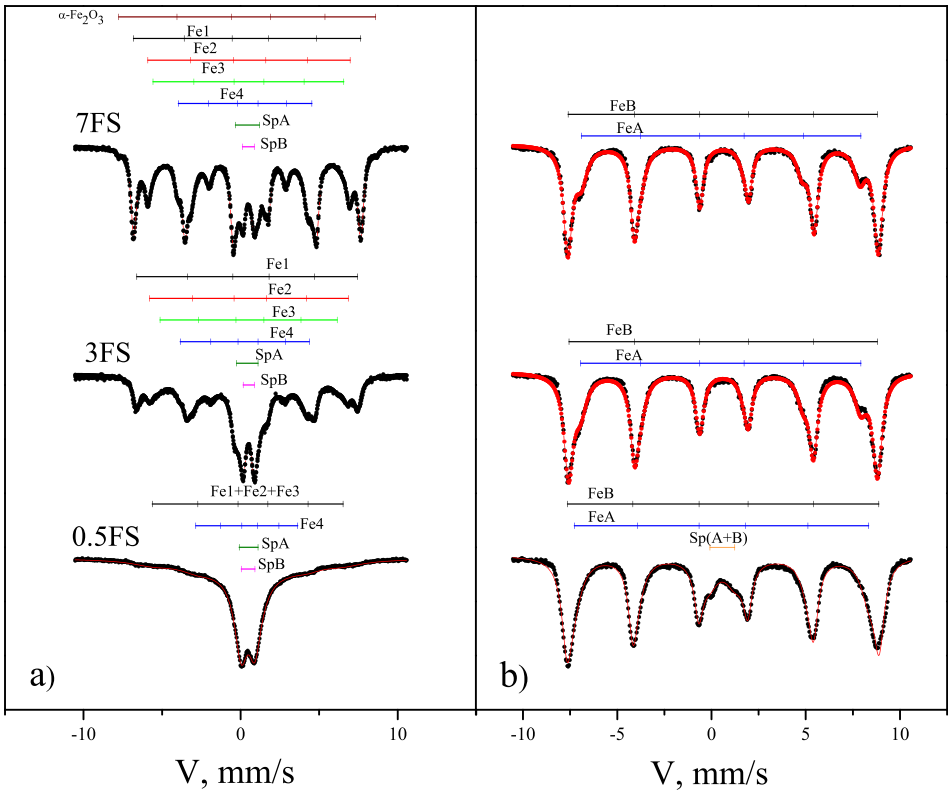

FIG. 2. Mössbauer spectra for samples 7FS, 3FS, and 05FS at temperatures of (a) 300 and (b) 4.2 K. Positions of absorption lines of subspectra are shown.

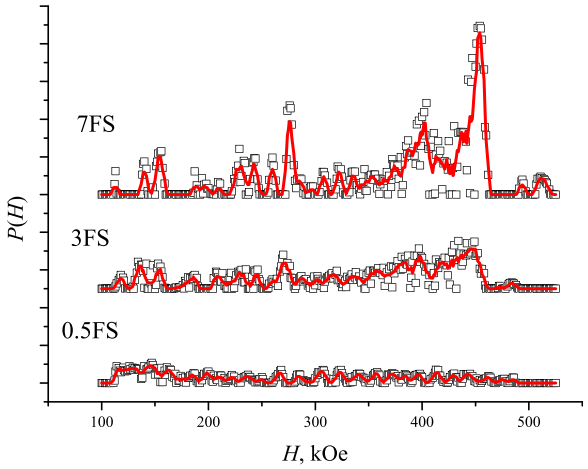

FIG. 3. Hyperfine field probability distribution on iron nuclei for samples 05FS, 3FS, and 7FS at room temperature.

crystallographic positions and mentioned the two limit cases: the ordered distribution, when the ratio between the numbers of occupied octahedral Fe(B) and tetrahedral Fe(A) positions is 3:1, and the disordered distribution, when this ratio is 3:2. The degree of ordering can probably depend on the oxide crystallization (synthesis) conditions and on the size of synthesized particles. We established that in the investigated samples the degree of ordering, i.e., the ratio $P_{Fe(B)}/P_{Fe(A)}$ between occupied positions, significantly depends on the iron content.

The average $P_{Fe(B)}/P_{Fe(A)}$ values are 2.85 ($P_{Fe(B)} = 0.74$ and $P_{Fe(A)} = 0.26$), 2.57 ($P_{Fe(B)} = 0.72$ and $P_{Fe(A)} = 0.28$), and 1.50 ($P_{Fe(B)} = 0.60$ and $P_{Fe(A)} = 0.40$) for samples 7FS, 3FS, and 05FS, respectively. Taking into account the identical sample preparation conditions and the histograms in Fig. 1, we may conclude that with decreasing particle size the ε-Fe_2O_3 oxide becomes increasingly disordered. The larger population of the tetrahedral positions in sample 05FS can result in changing of magnetic sublattices content, the exchange coupling between them, and in the observed enhancement of the effective magnetic moment per iron atom in this sample: $\sim 0.76\ \mu_B$ (Ref. 20) instead of $0.3\ \mu_B$ for coarse particles.[4,5,9,10]

As the relation of populations of octahedral cations to population of tetrahedral cations must be 3:1 in ε-Fe_2O_3 we can guess the 75% "trough" is related to the octahedral cations, as 25% are related to the tetrahedral ones. The same approximation was used for SP-phase of the 05FS sample at the liquid helium temperature. Consequently as the population, obtained from Mössbauer spectra, in all the iron cations in the sample is the same as in the ε-Fe_2O_3 structure, this is justified to determine the structure of the nanoparticles as ε-Fe_2O_3.

Let us consider a relative amount of iron atoms, which can be observed in the Mössbauer spectra in the form of quadrupole doublets characteristic of the SP state. At liquid helium temperature, the SP phase is observed only in sample 05FS in the amount of about 12%, which can correspond to particles smaller than 1.5 nm or to the surface iron atoms (see Section III F). At room temperature, the SP phase fraction in samples 7FS, 3FS, and 05FS increases to 11%, 24%, and 50% of the total iron amount, respectively.

B. FMR spectroscopy

Ferromagnetic resonance spectra detected at different temperatures are shown in Fig. 4. The spectra contain a

TABLE I. Mössbauer parameters for samples 0.5FS, 3FS, and 7FS. *IS* is the isomer chemical shift relative to α-Fe, *H* is the hyperfine field, *QS* is the quadrupole splitting, *W* is the linewidth, and *P* is the population of a position (area under partial spectrum).

	T = 300 K						T = 4.2 K					
sample	*IS* mm/s ± 0.005	*H* kOe ± 5	*QS* mm/s ± 0.02	*W* mm/s ± 0.02	*P* ± 0.05	Position	*IS* mm/s ± 0.005	*H* kOe ± 5	*QS* mm/s ± 0.02	*W* mm/s ± 0.02	*P* ± 0.05	Position
7FS	0.381	449	−0.44	0.37	0.28	Fe1	0.494	512	−0.13	0.46	0.70	Fe(B)
	0.384	400	−0.08	0.45	0.16	Fe2						
	0.354	378	−0.11	0.92	0.16	Fe3						
	0.347	…	0.73	0.49	0.09	SP(B)						
	0.210	265	−0.31	0.55	0.16	Fe4	0.353	459	−0.09	0.64	0.30	Fe(A)
	0.268		1.53	0.42	0.02	SP(A)						
	0.335			4.32	0.12	trough						
	0.402	512	−0.41	0.07	0.01	α-Fe_2O_3						
3FS	0.385	439	−0.49	0.45	0.17	Fe1	0.487	511	−0.10	0.51	0.69	Fe(B)
	0.393	393	−0.20	0.60	0.16	Fe2						
	0.390	352	−0.14	0.74	0.09	Fe3						
	0.359		0.71	0.50	0.18	SP(B)						
	0.215	256	−0.44	0.80	0.15	FeT	0.364	463	−0.12	0.68	0.31	Fe(A)
	0.294		1.36	0.62	0.06	SP(A)						
	0.221			6.44	0.19	trough						
0.5FS	0.466	378	−0.67	2.09	0.17	Fe1+Fe2+Fe3	0.468	514	−0.02	0.53	0.52	Fe(B)
	0.319		0.84	0.93	0.38	SP(B)						
	0.325	201	−0.36	3.57	0.29	Fe4	0.401	486	−0.11	0.88	0.36	Fe(A)
	0.368		1.22	1.31	0.12	SP(A)						
	0.154			1.98	0.04	trough	0.406		1.33	1.20	0.12	SP(A+B)

narrow high-intensity absorption line corresponding to particles in the SP state. The linewidth decreases in the series 7FS, 3FS, and 05FS, which is consistent with the well-known dependence of the magnetic resonance line width on the average particle size in the SP ensemble.[28] The ferromagnetic resonance spectra for the ensemble of magnetic particles with a specified size distribution were simulated using the model proposed by Berger *et al*. in Ref. 29. The approach used is based on temperature and size dependences of the FMR absorption linewidth of SP particles. Thermal fluctuations in the ensemble of SP particles lead to an effective decrease in the absorption linewidth by the expense of the local field anisotropy averaging. In the first approximation, after averaging over the SP particle ensemble, the absorption linewidth is described as $\Delta H = \Delta H_0 \cdot L(M_S HV/\mathrm{kT}) \cdot L(K_{\mathrm{eff}} V_{\max}/\mathrm{kT})$, where ΔH_0 is the linewidth of an individual non-SP particle, $L(x)$ is the Langevin function, M_S is the specific saturation magnetization of particles, V is the particle volume, K_{eff} is the effective magnetic anisotropy constant, and V_{max} is the volume of the largest particle in a sample. In the most general case, the absorption line can be written as

$$I(H) = \int_{\vartheta}\int_{\varphi}\int_{D} F(H, H_0(\vartheta, \varphi, D), \Delta H(D)) \times f_V(D) \sin\vartheta d\vartheta d\varphi dD, \quad (3)$$

where F(H, H_0, ΔH) is the line shape for an individual particle, $f_V(D)$ is the fraction of particles of a specified size in the sample, H_0 is the resonance field of an individual particle depending on the external magnetic field direction and particle size, and $\Delta H(D)$ is the linewidth of the SP ensemble of particles of a specified size.

The best agreement between the calculated and experimental spectra (Fig. 4) was obtained at $M_S = 20 \pm 5$ emu/g,[10] the effective magnetic anisotropy constant $K_{\mathrm{eff}} = 2 \times 10^6$ erg/cm^3, and the absorption linewidth for an individual particle $\Delta H_0 = 700$ Oe (the shape anisotropy was ignored). The log-normal particle size distributions were used, which describe well the experimental histograms (Fig. 1).[21] It should be noted that in the simulation we ignored temperature dependence of the magnetic anisotropy constant, the dependence of line shape from the particle shape distribution, and interparticle interactions. All the effects are difficult to account, and for the particular samples are supposed to be of the same order of magnitude. These simplifications can lead to deviations of the model spectra from real ones,[30] that in particular, case is especially noticeable for the sample 05FS. Another important circumstance is a significant FMR linewidth broadening at a temperature of 110 K in sample 7FS as compared with samples 3FS and 05FS. It means that at this temperature almost all particles in sample 7FS are blocked and do not exhibit the SP behavior in the FMR technique. This effect is considered in more detail in Section III D.

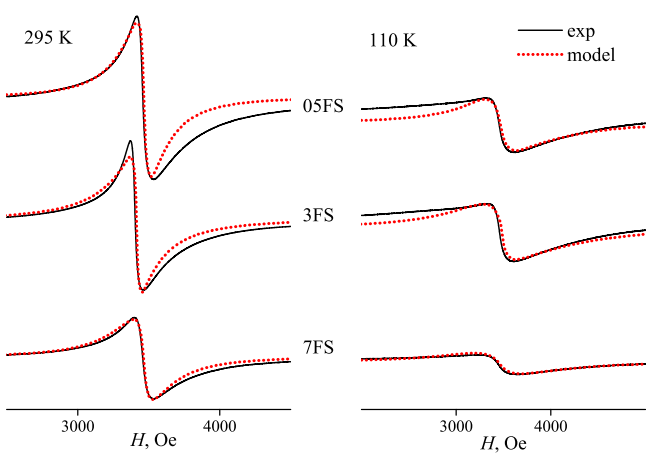

FIG. 4. Experimental (solid lines) and model (dotted lines, see Section III B, Eq. (3)) FMR spectra for the investigated samples at different temperatures.

C. Temperature dependences of magnetization

1. Temperature of the transition to the magnetically ordered state

Temperature dependences of the magnetic moment $M(T)$ measured on samples 7FS and 3FS under the ZFC and FC conditions are shown in Fig. 5 (the $M(T)$ dependences for sample 05FS are shown in the inset of Fig. 5). In these measurements, the filed cooling was performed at $H = 1$ kOe from 300 K to 4.2 K, and the high-temperature data were obtained in the ZFC regimes in the range of 300–600 K.

Now, let us consider the high-temperature data. The temperature of the transition of sample 7FS to the magnetically ordered state can be exactly established and amounts to ~510 K; i.e., at this temperature the curvature of the $M(T)$ dependence changes its sign. In addition, one can see a local maximum in the $M(T)$ dependence for this sample near 450 K, which was observed in Ref. 13 for rather coarse ε-Fe_2O_3 particles.

For sample 3FS, the temperature at which the curvature of the $M(T)$ dependence changes its sign in the high-temperature region is somewhat lower (470 K). In the wide

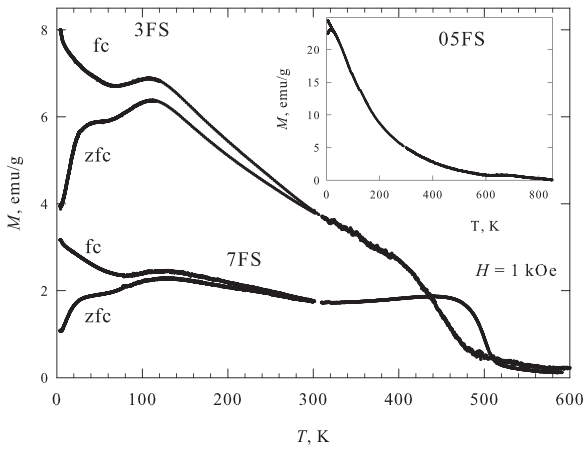

FIG. 5. Temperature dependences of the magnetic moment in the field $H = 1$ kOe at temperatures 4.2–600 K for samples 7FS and 3FS. ZFC and FC from 300 to 4.2 K. Inset: data for sample 05FS at temperatures of up to 850 K.

temperature range, the magnetic moment of this sample in the relatively weak external field $H = 1$ kOe is much higher than in sample 7FS. This indicates the presence of unblocked SP particles in sample 3FS. The functional $M(T)$ dependence of an unblocked particle is, as a rule, proportional to $1/T$, and the resulting temperature dependence of the magnetic moment for the entire ensemble of particles is more complex. This can cause the apparent reduction of the magnetic ordering temperature for sample 3FS. Sample 05FS containing the smallest particles exhibits the SP behavior up to temperatures of 800–850 K (inset of Fig. 5), which is confirmed by the temperature dependences of the integral intensity of FMR spectra.[20]

Thus, we may state that at least in particles larger than 6 nm (the maximum size of most particles in sample 05FS), the magnetic ordering temperature is ~500 K, which agrees well with the data reported in Refs. 2 and 3. The observed increase in the magnetic ordering temperature for sample 05FS can result from the magnetic order conservation up to high temperatures in small-particle fragments[20] and is apparently related to redistribution of iron atoms over crystallographic positions (see Section III A).

2. Magnetic transition in the temperature range 80–150 K

Let us consider the $M(T)$ dependences below room temperature. It can be seen in Fig. 5 that the $M(T)$ dependences of samples 7FS and 3FS behave differently under the FC and ZFC conditions at temperatures up to 300 K and contain maxima at 110–120 K. In sample 05FS, the effect of the thermomagnetic prehistory at $H = 1$ kOe manifests itself below ~35 K.

Figures 6(a)–6(c) show the behavior of the $M(T)$ dependences for the investigated samples in the low-temperature region at different thermomagnetic prehistories and external fields. In sample 7FS, the temperature of the $M(T)$ maximum (110–120 K) is field-independent (Fig. 6(a)) and therefore is not a temperature of blocking (magnetic-moment freezing) of the entire particle ensemble. The observed behavior is in satisfactory agreement with the experimental data for the samples containing ε-Fe_2O_3 particles 20–90 nm in size.[3,11,13] As is known, in the range 80–150 K, the ε-Fe_2O_3 oxide undergoes the magnetic transition, which manifests itself as a sharp decrease in the magnetic moment with decreasing temperature.[2,3,11,13] This behavior of the $M(T)$ dependences is observed in the FC and ZFC regimes for samples 7FS and 3FS at $H = 1$ kOe, which should be attributed to the magnetic transition in ε-Fe_2O_3.

In sample 05FS, most of ε-Fe_2O_3 particles are smaller than ~6 nm and, judging by the $M(T)$ dependences, which have no anomalies near 110–120 K (Fig. 6(c)), the magnetic transition does not occur in such particles. The authors of Ref. 13 considered the magnetic transition in the temperature range of 80–150 K to be an analog of the Morin point for a canted antiferromagnet. On the other hand, it is well-known that the Morin point of α-Fe_2O_3 particles decreases starting from a certain size[31] and is missing at a particle diameter of about 10 nm.[24] Probably, in our case we observed the

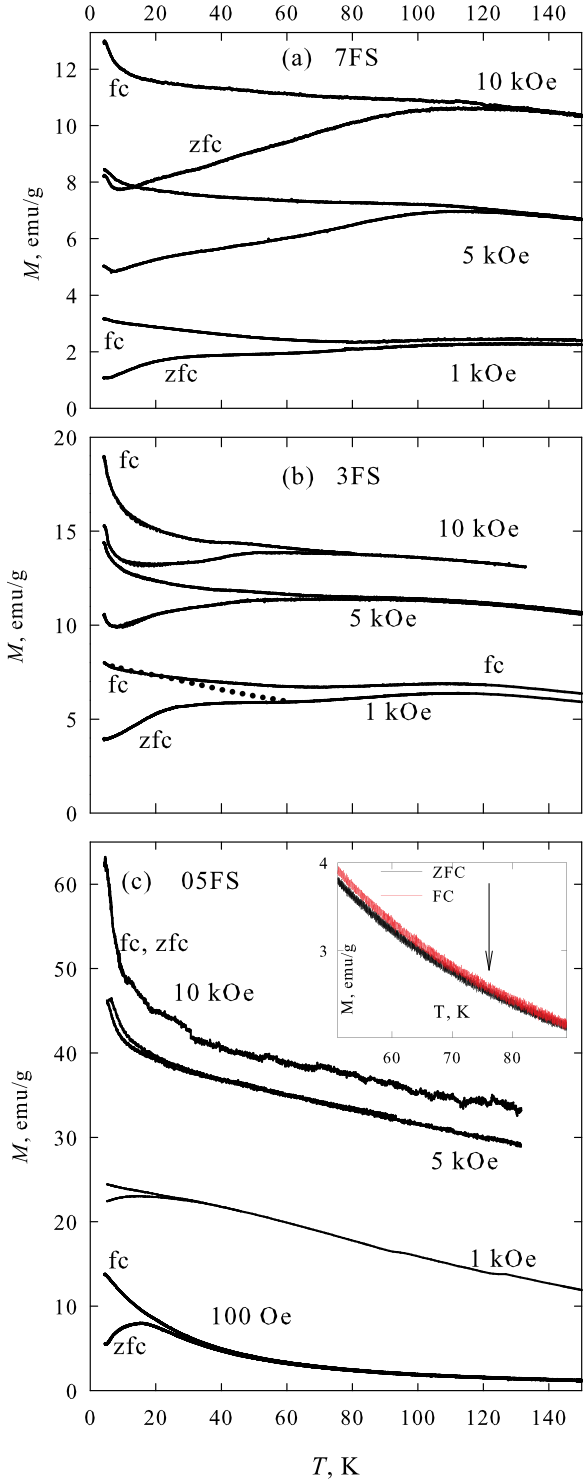

FIG. 6. $M(T)$ dependences at temperatures of up to 150 K under the ZFC and FC conditions in different magnetic fields for samples 7FS (a), 3FS (b), and 05FS (c). Dotted curve in (b) corresponds to $M(T)$ dependence upon FC conditions from 60 K at $H = 1$ kOe. Inset in (c): $M(T)$ dependences for sample 05FS upon ZFC and FC in the field $H = 100$ Oe. The arrow indicates the temperature of irreversible behavior of the $M(T)$ dependence.

analogous behavior: in sample 05FS with ε-Fe_2O_3 particles smaller than ~6 nm, the magnetic transition temperature shifted at least below 4.2 K. Redistribution of cations over crystallographic positions with decreasing particle size (see Section III A) can also be caused by the absence of magnetic transition in particles smaller than 6 nm.

D. Blocking temperature in different techniques. The role of surface anisotropy

The strong influence of an external field on the temperature of the $M(T)$ maximum in the ZFC regime and on the temperature of irreversible magnetization behavior in systems of small particles indicates blocking of magnetic moments of these particles. This is especially pronounced for sample 05FS, which can be seen in Fig. 6(c) presenting the $M(T)$ dependences under the ZFC and FC conditions at different external fields. The inset to Fig. 6(c) shows details of the $M(T)$ dependences for sample 05FS upon ZFC and FC in the field $H = 100$ Oe. It is seen that the temperature at which the ZFC and FC $M(T)$ dependences coincide is ~75 K and, logically, it corresponds to the temperature of blocking of the largest (~6 nm) particles in sample 05FS.

Samples 3FS and 7FS also contain a large fraction of particles smaller than 6 nm (Figs. 1(a) and 1(b)). The blocking of such particles can be observed in the form of plateaus in the $M(T)$ dependences in the range 30–70 K (Figs. 5(a) and 5(b)). The behavior of the $M(T)$ dependence at $H = 1$ kOe under FC conditions starting from the intermediate temperature $T = 60$ K (Fig. 5(b)), specifically, the growth of magnetic moment with decreasing temperature confirms the blocking of small particles at low temperatures.

The authors of study[4] reported a magnetic anisotropy constant of $\sim 5 \times 10^6$ erg/cm^3 at room temperature for ε-Fe_2O_3 particles ~25 nm in size. Ignoring the surface anisotropy contribution at this K_V value, we obtain from Eq. (1) that the blocking temperature for particles with $D \approx 6$ nm should be 280 K. This is much higher than the temperature of irreversible behavior of magnetic moment at $H = 100$ Oe (~75 K, inset of Fig. 6(c)). Moreover, according to the data reported in Ref. 4, the bulk magnetic anisotropy near 80 K is only $\sim 10^2$–10^3 erg/cm^3 and such a sharp drop of K_V results from the magnetic transition in ε-Fe_2O_3 at temperatures of 80–150 K. However, the results presented in Section III C allow us to conclude that in 6 nm particles the magnetic transition does not occur. Consequently, the values and temperature evolutions of the magnetocrystalline anisotropy constant are strongly different for small and large ε-Fe_2O_3 particles.

As was shown in Section III A, in ε-Fe_2O_3 nanoparticles smaller than 10 nm, one can observe the iron cation distribution over crystallographic positions different from the ordered distribution typical of relatively coarse (25 nm) nanoparticles. In addition, according to expression (2), in such small particles the surface magnetic anisotropy will make a significant contribution. Therefore, it is interesting to determine the dependence of the effective anisotropy constant on particle size from the data obtained using different techniques and estimate the crystallographic and surface magnetic anisotropy constants for the disordered state of the ε-Fe_2O_3 oxide phase. In the analysis presented below, we consider in the first approximation that particles have a cubic shape.

In the ferromagnetic resonance spectra for sample 05FS and, to a lesser extent, for sample 3FS, at a temperature of 110 K (Fig. 4) one can observe not only a wide nonuniformly broadened signal but also a narrow line corresponding to unblocked particles that exhibit the SP behavior. The integral intensity of this line amounts to 10% of the total intensity.

The changes of FMR spectra observed with the temperature decreasing in principle might be of different origin.[32,33] In this particular case, the widening of the resonance line is observed that is typical for the nanoparticles that transit from the superparamagnetic regime. At the same time, the total integral intensity remains constant. The situation is appeared to be complex due to the overlapping of different phenomena. The magnetic transition is observed for ε-Fe_2O_3 nanoparticles at T = 80–150 K (Refs. 3 and 4) that leads to the changes of the magnetic properties resulting in the decrease of the FMR spectra intensity.[32] However, we do not see any significant shift of the resonance field. It means that the alteration of crystallographic anisotropy in this temperature range along could not explain the spectra changes observed. At the same time, the transition from the superparamagnetic regime can increase the spectra intensity and the width.[33] So the interference of these two effects results in the preservation of the total integral intensity and the widening of the spectra observed.

Since the SP behavior is typical of the smallest particles in a sample, we can calculate the particle size at which the blocking temperature is ~110 K by comparing the particle size distributions. At the transition from samples 05FS and 3FS to sample 7FS, the average particle size significantly increases. We may conclude that this also leads to a decrease in the fraction of the smallest particles in this sample. In accordance with the histograms in Fig. 1, a good estimate for the size of the smallest of observed particles in the samples under study is 1.5 nm. In other words, the particles 1.5 nm in size and smaller exhibit the SP behavior in the FMR experiment at 110 K and the blocking temperature of these particles is ~110 K. Indeed, if, according to Ref. 34, the estimate for the FMR technique is $\tau_0 = \pi/(\gamma \cdot H_0) \approx 5 \times 10^{-11}$ s, where γ is the gyromagnetic ratio and H_0 is the resonance field, then the effective anisotropy constant obtained from Eq. (1) for a critical particle size of 1.5 nm is 3×10^6 erg/cm^3.

In addition, the magnetic measurements yield $T_B \approx 75$ K for the size $D \approx 6$ nm (irreversible behavior of the $M(T)$ dependences) and, if the $M(T)$ maximum temperature in the ZFC regime at $H = 100$ Oe is assumed to be a blocking temperature for particles of average size in sample 05FS, then we have $T_B \approx 15$ K for particles with $D \approx 3.1$ nm. In the static magnetic measurements, the values $\tau_{sm} \sim 10^1$–10^2 s and τ_0 are strongly different and the τ_0 value is not critical for determination of K_{eff} from (1). At $\tau_0 \approx 5 \times 10^{-11}$ s, we obtain $K_{eff} \approx 1.4 \times 10^6$ erg/cm^3 at $D \approx 6$ nm and $K_{eff} \approx 2 \times 10^6$ erg/cm^3 at $D \approx 3.1$ nm.

Figure 7 shows the K_{eff} values as a function of $1/D$ obtained from the FMR data and magnetic measurement data. It can be seen that this dependence is satisfactorily described by a linear function in accordance with (2). In addition, Fig. 7 presents the K_{eff} values obtained from the Mössbauer spectra analysis.

As was mentioned in Section III A, the approximate ratios between the sextet and doublet intensities in the Mössbauer spectra at room temperature can be determined. These ratios

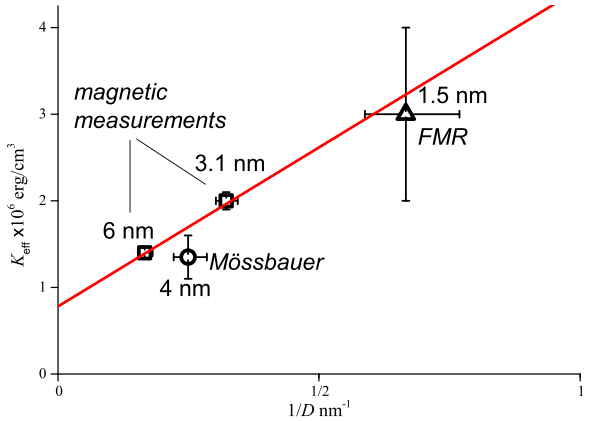

FIG. 7. Effective magnetic anisotropy constant vs inverse particle size for different experimental techniques (see Section III D). The straight line indicates data processing by dependence (2).

are 11%, 24%, and 50%, i.e., approximately correspond to the volume fractions of all particles with a size of less than ~4 nm (see the histograms in Fig. 1). Thus, in Mössbauer spectroscopy the size $D \sim 4$ nm can be considered critical for the SP state of ε-Fe_2O_3 particles at $T \approx 300$ K. However, determination of K_{eff} with the use of the Mőssbauer technique can be critical to the values $\tau_M \sim 10^{-9}$–10^{-8} s and τ_0. In addition, the temperature $T_B \approx 300$ K for the obtained size $D \approx 4$ nm is much higher than in the previous cases and the obtained K_{eff} value can be affected by the temperature dependence of the magnetic anisotropy constants. The value $K_{eff} \approx 1.35 \times 10^6$ erg/cm^3 for the size $D \approx 4$ nm (Fig. 7) was obtained at $\tau_M \sim 10^{-9}$ s and $\tau_0 \approx 5 \times 10^{-11}$ s (the same value was used in the FMR technique). It can be seen that the K_{eff} value for the Mössbauer technique is also in satisfactory agreement with the data obtained using the other methods.

It follows from the data illustrated in Fig. 7 that, according to Eq. (2), the bulk and surface anisotropy constants are $K_V \approx 7.8 \pm 0.2 \times 10^5$ erg/cm^3 and $K_S \approx 0.06 \pm 0.01$ erg/cm^2, respectively. Note that here we speak about ε-Fe_2O_3 particles smaller than ~6 nm. The bulk magnetic anisotropy constant for such particles is much smaller than for coarse particles[4] and there is apparently no strong temperature dependence of K_V. Concerning the surface anisotropy constant, in this analysis we assumed the K_S value to be weakly dependent on temperature. The obtained value $K_S \approx 0.06$ erg/cm^2 is consistent with the results reported in Ref. 21, where K_S was obtained from the analysis of dynamic hysteresis in sample 7FS. The surface magnetic anisotropy makes the main contribution to K_{eff} for small particles; e.g., for particles 3–6 nm in size, the K_{eff} value lies in the range $(1–3) \times 10^6$ erg/cm^3, which is close to the estimates made at the low (4.2 K) and high (300 K) temperatures for a particle size of ~25 nm.[4]

E. Estimation of the paramagnetic contribution

In the $M(T)$ dependences presented in Figs. 6(a)–6(c), one can see one more feature, specifically, an increase in the magnetic moment with decreasing temperature in the low-temperature range. This behavior is especially pronounced in the field $H = 10$ kOe (see Fig. 8) and is approximately identical for the FC and ZFC regimes at the identical fields. This indicates the contribution of either the paramagnetic subsystem or the smallest SP particles with a blocking temperature below 4.2 K. The contribution of this additional subsystem can be observed in the $M(H)$ dependences: at liquid helium temperature in sufficiently strong fields, the magnetic moment grows and saturates in a field of ~60 kOe, but with increasing temperature this behavior is not bright (Figs. 9(a)–9(c)). It can be seen that this contribution is especially pronounced in sample 05FS (Fig. 6(c)).

The analysis of the described behavior of the $M(T)$ dependences (Figs. 6(a)–6(c) and 8) and $M(H)$ dependences (Figs. 9(a)–9(c)) showed that this additional contribution is described in the best way by the presence of a paramagnetic subsystem. The paramagnetic contribution for the investigated sample series was estimated by subtracting the function $M_{PM} \times B(H,T)$ from the experimental $M(H,T)$ data (M_{PM} is the paramagnetic contribution in emu/g and $B(H,T)$ is the Brillouin function for the Fe^{3+} atom spin equal to 5/2 and g factor equal to 2). The criterion of validity of the estimation was the assumption that for the SP system the FC M(T) dependence at temperatures below the blocking temperature (the $M(T)$ maximum in the ZFC regime) weakly changes and the ZFC M(T) dependence is an increasing function. In addition, we took into account the $M(H)$ dependences in the low-temperature region (Figs. 9(a)–9(c)). Figure 8 presents the results of subtraction of the paramagnetic component from the M(T) data for the samples under study. Comparison with the initial data shows the modification of the $M(T)$ dependences with the paramagnetic contribution involved. In addition, Fig. 8 shows the contribution of the paramagnetic subsystem at $H = 10$ kOe for the investigated

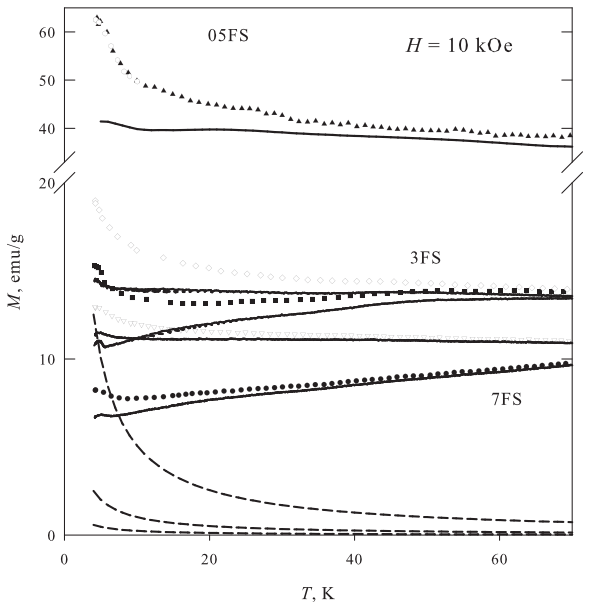

FIG. 8. Initial $M(T)$ dependences for samples 7FS, 3FS, and 05FS in the field $H = 10$ kOe under the ZFC (closed symbols) and FC (open symbols) conditions and the results of subtraction of the paramagnetic contribution (solid curves) from these dependences. The paramagnetic contribution in the field $H = 10$ kOe is shown by dotted curves (for samples 05FS, 3FS, and 7FS downwards).

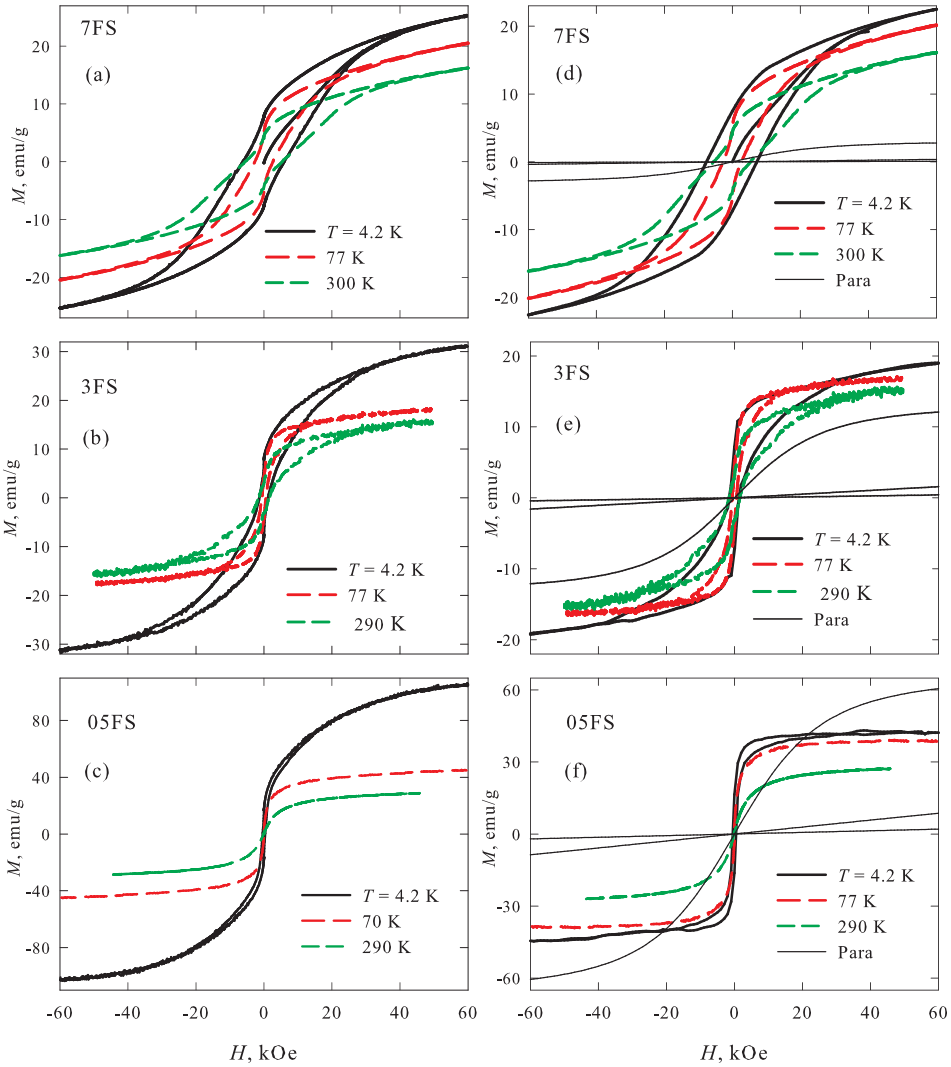

FIG. 9. $M(H)$ dependences for samples 7FS ((a), (d)), 3FS ((b), (e)), and 05FS ((c), (f)) at different temperatures. Initial $M(H)$ data are shown in (a)–(c). Results of subtraction of the paramagnetic contribution $M_{PM} \times B(H,T)$ and the paramagnetic component (dotted curves) are shown in (d)–(f). The M_{PM} values are presented in Section III E. The scales along the Y axis in ((a), (d)), ((b), (e)), and ((c), (f)) are different.

samples. The results of the analogous subtraction of the paramagnetic contribution from the initial $M(H)$ dependences and the paramagnetic contribution in itself are illustrated in Figs. 9(d)–9(f). Comparing the data presented in Figs. 9(d)–9(f) with the data in Figs. 9(a)–9(c) for samples 7FS, 3FS, and 05FS, one can see how the account for the paramagnetic contribution modifies the $M(H)$ dependences. Note that the analogous processing of the initial data under the assumption of SP behavior of the smallest (below 1.5 nm) particles, which can be unblocked at 4.2 K, does not yield satisfactory agreement in neither the $M(T,H)$ dependences nor the contribution of the additional subsystem.

It was found that the M_{PM} values are 65 ± 5, 13 ± 2, and 3 ± 2 emu/g for samples 05FS, 3FS, and 7FS, respectively. This corresponds to ~20% (05FS), ~4%(3FS), and ~1%(7FS) of the total iron amount in particles and, taking into account the histograms (Fig. 1), we may conclude that the paramagnetic contribution is typical of the smallest particles. It would be reasonable to suggest that paramagnetism is caused by surface iron atoms with unsaturated chemical bonds. Taking the average distance between Fe^{3+} atoms to be ~3.1 Å,[13] we obtain that under the assumption of the cubic particle shape, the fractions of paramagnetic atoms are ~50% (05FS), ~18%(3FS), and ~8%(7FS) of the total amount of surface iron atoms. The obtained values correspond to the total surface of particles smaller than 3.5–4 nm for all the investigated samples.

According to the Mössbauer spectra (Table I), at $T = 4.2$ K the quadrupole doublets characteristic of the SP state of particles or the paramagnetic behavior of separate atoms (about 12% of the total amount of iron in the sample) are observed only in sample 05FS (see Section III A). The discrepancy between this value and the magnetic measurement data (20%) is apparently related to the partial spin-glass-like behavior of this paramagnetic subsystem. Indeed, the spin-glass-like behavior of surface atoms in magnetically ordered nanoparticles is met fairly often[35–38] and is usually observed in the form of anomalies in the $M(T)$ dependence under the FC conditions below the particle blocking temperature. Sometimes, as in our case, the paramagnetic behavior of surface atoms is observed.[39,40] In addition, the spin-glass-like state has a characteristic relaxation time determined by the local environment of a spin. In the magnetic measurements of the investigated samples with the characteristic time $\tau_{sm} \sim 10^1$–10^2 s, the surface of small particles behaves like a classical paramagnetic subsystem. In Mössbauer spectroscopy ($\tau_M \sim 10^{-9}$–10^{-8} s), this subsystem can partially exhibit the spin-glass-like behavior, which is indicated by a wide hyperfine field distribution in Fig. 3.

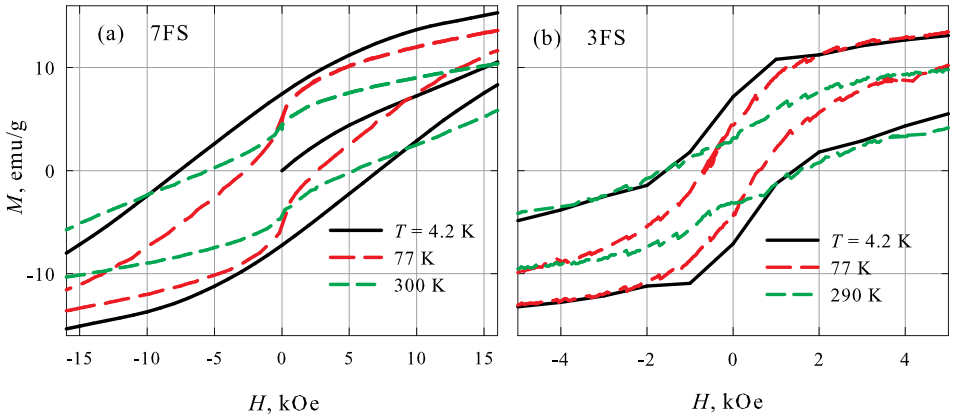

FIG. 10. Portions of the hysteresis $M(H)$ dependences for samples 7FS and 3FS at different temperatures.

Thus, the paramagnetic contribution observed in the static magnetic measurements and increasing in the sample series 7FS, 3FS, and 05FS is caused by the surface iron atoms of the smallest particles.

F. Hysteresis M(H) dependences

The $M(H)$ dependences for samples 3FS and 7FS show the hysteresis over the entire temperature range from 4.2 to 300 K (Figs. 9(a) and 9(b)). Taking into account the paramagnetic contribution (Figs. 9(d) and 9(e)), we may state that the $M(H)$ dependences for samples 3FS and 7FS are similar to the data for rather coarse (~25 nm) ε-Fe_2O_3 particles.[2–4] The field of the irreversible behavior of the $M(H)$ dependence is more than 40 kOe and the magnetic moment in strong fields is ~15–20 emu/g. Nevertheless, coercivity H_C (~20 kOe at room temperature[2–5]) does not take large values, as can be seen in Fig. 10 presenting portions of the hysteresis $M(H)$ dependences for samples 3FS and 7FS near $M \sim 0$. In these samples, there is a significant fraction of particles smaller than 6 nm (Fig. 1), which are unblocked in a wide temperature range (see Section III D). Magnetization curves for these small particles are fully reversible in a wide temperature range, which is confirmed by the experimental $M(H)$ data for sample 05FS, (Figs. 9(c) and 9(f) (in this sample, $H_C = 0$ at temperatures above ~40 K). If at some temperature T the sample contains a mixture of blocked ($K_{eff}V/25\,k > T$) and unblocked ($K_{eff}V/25\,k < T$) particles, then the resulting $M(H)$ dependence is a superposition of additive contributions from the hysteresis dependences (for blocked particles) and the Langevin function with regard to the size distribution of magnetic moments (for SP particles). In this case, coercivity H_C can significantly decrease depending on the fraction of SP particles.

The H_C values for the investigated samples at different temperatures are shown in Fig. 11. For comparison, Fig. 11 shows the data for coarse (~25 nm) ε-Fe_2O_3 particles from study.[4] One can see the described difference in the H_C values for the investigated samples at $T = 300$ K. In particular, H_C of sample 7FS at $T = 300$ K attains 5.6 kOe; in sample 3FS, the fraction of SP particles is larger and $H_C(T = 300\,K)$ is merely 1.7 kOe, whereas for coarse particles the coercivity is $H_C \approx 20$ kOe.[4] In the vicinity of 80 K, the H_C values noticeably decrease due to a decrease in the bulk magnetic anisotropy constant of ε-Fe_2O_3 after the magnetic transition. In the low-temperature region, H_C somewhat increases, which can be related either to the growth of the bulk magnetic anisotropy constant or to the effect of surface anisotropy. The temperature behavior of H_C for samples 7FS and 3FS is nonmonotonic, which is typical of coarse particles. Sample 05FS reveals no features characteristic of the magnetic transition in ε-Fe_2O_3; therefore, H_C monotonically decreases to zero with increasing temperature (Fig. 10(c)). This sample exhibits the twice higher magnetic moment in strong fields (~40 emu/g at $T = 4.2$ K) and effective magnetic moment per iron atom (~0.76μ_B),[20] which is consistent with the observed redistribution of cation positions with decreasing particle size (see Section III A).

Note that at the temperature $T = 77$ K the H_C value for sample 7FS ($H_C \approx 2.65$ kOe) is somewhat higher than the value for particles ~25 nm in size ($H_C \approx 1.5$ kOe), which can be related to the surface anisotropy contribution. Indeed, the K_V value near ~80 K is only ~10^3 erg/cm^3 (Ref. 4) and even for sufficiently large particles ($D \sim 25$ nm) the surface anisotropy at the above-estimated value $K_S \sim 0.06$ erg/cm^2 yields the K_{eff} value (~10^5 erg/cm^3) that is higher by two orders of magnitude, which results in a small yet nonzero H_C. Since in the first approximation we have $H_C \sim K_{eff}$ (Ref. 41), then for particles ~10 nm in size (about $\langle D \rangle$ for sample 7FS), we can

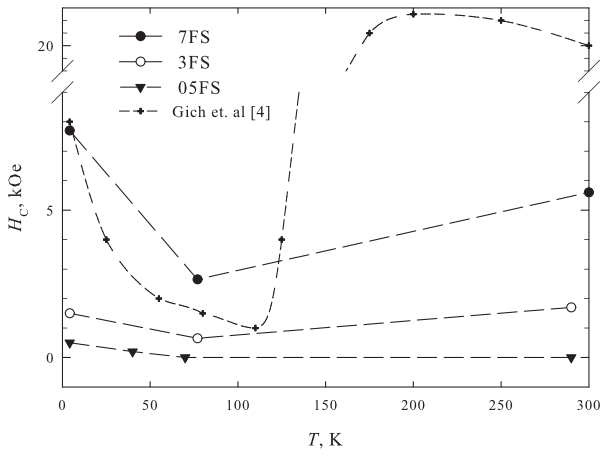

FIG. 11. Temperature dependence of coercivity H_C for the investigated samples. Data for ε-Fe_2O_3 particles ~25 nm in size from study[4] are also shown.

expect at least a doubled H_C value (as compared with the case $D \sim 25$ nm), which is observed in sample 7FS at $T \sim 80\,K$ as compared with the data from Ref. 4.

IV. CONCLUSIONS

Magnetic properties of ε-Fe_2O_3 nanoparticles with different average sizes (3–9 nm) and dispersions deposited on silica gel were studied. According to the Mössbauer spectroscopy data, the samples, including those with particles smaller than 6 nm, are characterized by the parameters of the ε-Fe_2O_3 structure.

The presence of particles ~10–25 nm in size in samples 3FS and 7FS leads to the features in the magnetic properties which are characteristic to of ε-Fe_2O_3 phase, specifically, the transition to the magnetically ordered state (~500 K), nonmonotonic temperature behavior of coercivity, and anomalies accompanying the magnetic transition at 80–150 K.

Meanwhile, the particles smaller than 6 nm behave differently. The temperature of the transition to the magnetically ordered state significantly increases (to ~800 K) and the magnetic transition does not occur. In addition, it was found that the bulk magnetic anisotropy constant for small particles is strongly different from the K_V values typical of particles about 20 nm in size at $T = 300$ K.

As the particle size decreases to the value $D \sim 6$ nm, the Mössbauer spectra indicate redistribution of cation positions: population of the tetrahedral positions significantly increases. This is consistent with the observed modification of the magnetic properties with decreasing ε-Fe_2O_3 particle size.

The Mössbauer and FMR spectroscopy data and the results of the static magnetic measurements indicated the superparamagnetic state of a certain fraction of particles at given temperature in each sample. Using the obtained data, we estimated the critical size of particles that behave superparamagnetically in different experimental techniques and determined the corresponding effective magnetic anisotropy constants.

This allowed us to extract the contributions of the bulk and surface magnetic anisotropies in small particles. For particles smaller than $D \approx 6$ nm, the K_V and K_S values were found to be $\sim 8 \times 10^5$ and $\sim 0.06 \pm 0.01$ erg/cm^2, respectively. Thus, the surface magnetic anisotropy dominates in the effective magnetic anisotropy of small particles.

It was found that surface atoms in small (<4 nm) particles behave like a paramagnetic subsystem in static magnetic measurements and its contribution increases in the series 7FS, 3FS, and 05FS. However, according to the Mössbauer spectroscopy data, we may speak about the partial spin-glass-like behavior of this subsystem.

ACKNOWLEDGMENTS

We are grateful to Professor Yu. L. Raikher for useful discussions and M. A. Kazakova for the help in sample preparation.

This work was supported by Russian Federal Agency of Scientific Organizations (Project No. V.44.1.15) and scientific and educational center of energy-efficient catalysis of NSU.

[1]E. Tronc, C. Chaneac, and J. P. Jolivet, J. Solid State Chem. **139**(1), 93 (1998).
[2]L. Machala, J. Tucek, and R. Zboril, Chem. Mater. **23**, 3255 (2011).
[3]J. Tucek, R. Zboril, A. Namai, and S. Ohkoshi, Chem. Mater. **22**, 6483 (2010).
[4]M. Gich, A. Roig, C. Frontera, E. Molins, J. Sort, M. Popovici, G. Chouteau, D. Martın y Marero, and J. Nogues, J. Appl. Phys. **98**(4), 044307 (2005).
[5]S. Ohkoshi, S. Sakurai, J. Jin, and K. Hashimoto, J. Appl. Phys. **97**, 10K312 (2005).
[6]M. Gich, C. Frontera, A. Roig, J. Fontcuberta, E. Molins, N. Bellido, Ch. Simon, and C. Fleta, Nanotechnology **17**, 687 (2006).
[7]S. Ohkoshi, S. Kuroki, S. Sakurai, K. Matsumoto, K. Sato, and S. Sasaki, Angew. Chem. Int. Ed. **46**, 8392 (2007).
[8]M. Yoshikiyo, A. Namai, M. Nakajima, K. Yamaguchi, T. Suemoto, and S. Ohkoshi, J. Appl. Phys. **115**, 172613 (2014).
[9]E. Tronc, C. Chaneac, J. P. Jolivet, and J. M. Greneche, J. Appl. Phys. **98**, 053901 (2005).
[10]Y. C. Tseng, N. M. Souza-Neto, D. Haskel, M. Gich, C. Frontera, A. Roig, M. van Veenendaal, and J. Nogues, Phys. Rev. B **79**(9), 094404 (2009).
[11]S. Sakurai, J. Jin, K. Hashimoto, and S. Ohkoshi, J. Phys. Soc. Jpn. **74**(7), 1946–1949 (2005).
[12]S. Sakurai, S. Kuroki, H. Tokoro, K. Hashimoto, and S. Ohkoshi, Adv. Funct. Mater. **17**, 2278 (2007).
[13]M. Kurmoo, J.-L. Rehspringer, A. Hutlova, C. D'Orlans, S. Vilminot, C. Estournes, and D. Niznansky, Chem. Mater. **17**, 1106 (2005).
[14]A. Namai, S. Sakurai, M. Nakajima, T. Suemoto, K. Matsumoto, M. Goto, S. Sasaki, and S. Ohkoshi, J. Am. Chem. Soc. **131**, 1170 (2009).
[15]A. I. Dmitriev, O. V. Koplak, A. Namai, H. Tokoro, S. Ohkoshi, and R. B. Morgunov, Phys. Solid State **55**(11), 2252–2259 (2013).
[16]A. I. Dmitriev, O. V. Koplak, A. Namai, H. Tokoro, S. Ohkoshi, and R. B. Morgunov, Phys. Solid State **56**(9), 1795–1798 (2014).
[17]G. A. Bukhtiyarova, O. N. Martyanov, S. S. Yakushkin, M. A. Shuvaeva, and O. A. Bayukov, Phys. Solid State **52**, 826 (2010).
[18]G. A. Bukhtiyarova, M. A. Shuvaeva, O. A. Bayukov, S. S. Yakushkin, and O. N. Martyanov, J. Nanopart. Res. **13**(10), 5527–5534 (2011).
[19]S. S. Yakushkin, A. A. Dubrovskiy, D. A. Balaev, K. A. Shaykhutdinov, G. A. Bukhtiyarova, and O. N. Martyanov, J. Appl. Phys. **111**(4), 044312 (2012).
[20]D. A. Balaev, A. A. Dubrovskiy, K. A. Shaykhutdinov, O. A. Bayukov, S. S. Yakushkin, G. A. Bukhtiyarova, and O. N. Martyanov, J. Appl. Phys. **114**, 163911 (2013).
[21]D. A. Balaev, I. S. Poperechny, A. A. Krasikov, K. A. Shaikhutdinov, A. A. Dubrovskiy, S. I. Popkov, A. D. Balaev, S. S. Yakushkin, G. A. Bukhtiyarova, O. N. Martyanov, and Yu. L. Raikher, J. Appl. Phys. **117**, 063908 (2015).
[22]I. S. Poperechny, Yu. L. Raikher, and V. I. Stepanov, Phys. Rev. B **82**, 174423 (2010).
[23]I. S. Poperechny and Yu. L. Raikher, Physica B **435**, 58–61 (2014).
[24]S. Mørup, D. E. Madsen, C. Frandsen, C. R. H. Bahl, and M. F. Hansen, J. Phys.: Condens. Matter **19**, 213202 (2007).
[25]F. Bødker, S. Mørup, and S. Linderoth, Phys. Rev. Lett. **72**(N2), 282 (1994).
[26]S. S. Yakushkin, G. A. Bukhtiyarova, and O. N. Martyanov, J. Struct. Chem. **54**(N.5) 876 (2013).
[27]A. D. Balaev, Yu. V. Boyarshinov, M. M. Karpenko, and B. P. Khrustalev, Prib. Tekh. Eksp. **3**, 167 (1985).
[28]R. S. de Biasi and T. S. Devezas, J. Appl. Phys. **49**, 2466 (1978).
[29]R. Berger, J. Kliava, J.-C. Bissey, and V. Baïetto, J. Appl. Phys. **87**, 7389 (2000).
[30]E. de Biasi, C. A. Ramos, and R. D. Zysler, "Size and anisotropy determination by ferromagnetic resonance in dispersed magnetic nanoparticle systems," J. Magn. Magn. Mater. **262**(2), 235–241 (2003).
[31]N. Amin and S. Arajs, Phys. Rev. B **35**, 4810 (1987).
[32]E. De Biasi, E. Lima, Jr., C. A. Ramos, A. Butera, and R. D. Zysler, "Effect of thermal fluctuations in FMR experiments in uniaxial magnetic nanoparticles: Blocked vs. superparamagnetic regimes," J. Magn. Magn. Mater. **326**, 138–146 (2013).
[33]R. Berger, J. Kliava, J.-C. Bissey, H. Daubric, and C. Estournes, "Temperature dependence of superparamagnetic resonance of iron oxide nanoparticles," J. Magn. Magn. Mater. **234**, 535–544 (2001).
[34]J. L. Dormann, D. Fiorani, and E. Tronc, "Magnetic relaxation in fine-particle systems," in *Advances in Chemical Physics*, edited by I. Prigogine and S. A. Rice (John Wiley & Sons, Inc., Hoboken, NJ, USA, 1997), Vol. 98.

[35]B. Martınez, X. Obradors, L. Balcells, A. Rouanet, and C. Monty, Phys. Rev. Lett. **80**(N1), 181 (1998).
[36]R. H. Kodama and A. E. Berkowitz, Phys. Rev. B **59**, 6321 (1999).
[37]Yu. A. Koksharov, S. P. Gubin, I. D. Kosobudsky, G. Yu. Yurkov, D. A. Pankratov, L. A. Ponomarenko, M. G. Mikheev, M. Beltran, Y. Khodorkovsky, and A. M. Tishin, Phys. Rev. B **63**, 012407 (2000).
[38]K. Nadeem, H. Krenn, T. Traussnig, R. Würschum, D. V. Szabo, and I. Letofsky-Papst, J. Appl. Phys. **111**, 113911 (2012).
[39]E. Winkler, R. D. Zysler, and D. Fiorani, Phys. Rev. B **70**, 174406 (2004).
[40]X. Chen, S. Bedanta, O. Petracic, W. Kleemann, S. Sahoo, S. Cardoso, and P. P. Freitas, Phys. Rev. B **72**, 214436 (2005).
[41]E. C. Stoner and E. P. Wohlfarth, Philos. Trans. R. Soc. London, Ser. A **240**, 599 (1948).